

Typicality at quantum-critical points

Lu Liu,¹ Anders W. Sandvik,^{2,3,*} and Wenan Guo^{1,†}

¹*Department of Physics, Beijing Normal University, Beijing 100875, China*

²*Department of Physics, Boston University, 590 Commonwealth Avenue, Boston, Massachusetts 02215*

³*Beijing National Laboratory for Condensed Matter Physics and Institute of Physics, Chinese Academy of Sciences, Beijing 100190, China*

We discuss the concept of typicality of quantum states at quantum-critical points, using projector Monte Carlo simulations of an $S = \frac{1}{2}$ bilayer Heisenberg antiferromagnet as an illustration. With the projection (imaginary) time τ scaled as $\tau = aL^z$, L being the system length and z the dynamic critical exponent (which takes the value $z = 1$ in the bilayer model studied here), a critical point can be identified which asymptotically flows to the correct location and universality class with increasing L , independently of the prefactor a and the initial state. Varying the proportionality factor a and the initial state only changes the cross-over behavior into the asymptotic large- L behavior. In some cases, choosing an optimal factor a may also lead to the vanishing of the leading finite-size corrections. The observation of typicality can be used to speed up simulations of quantum criticality, not only within the Monte Carlo approach but also with other numerical methods where imaginary-time evolution is employed, e.g., tensor network states, as it is not necessary to evolve fully to the ground state but only for sufficiently long times to reach the typicality regime.

I. INTRODUCTION

Typicality in quantum many-body physics refers to the emergence in large systems of typical properties of arbitrary pure states that depend only on global control variables such as the energy.^{1–3} If an observable is typical, details of the initial state preparation in an experiment do not matter. The perhaps most striking example of typicality is the eigenstate thermalization hypothesis (ETH),^{4–6} according to which a single eigenstate suffices to characterize the properties of a statistical ensemble of states at the temperature corresponding to the energy. The ETH and other manifestations of typicality are now believed to hold generically, but with important exceptions in, e.g., integrable systems.^{7,8}

The concept of typicality is at the heart of fundamentally understanding how macroscopic properties emerge from the microscopic scale in quantum systems. It is also of practical interest experimentally, especially as deviations from typicality become important in nano-scale systems. With the increasing importance of numerical simulations in quantum many-body physics for systems that are analytically intractable, the issue of typicality is also of key importance both in interpreting simulation results and for setting up simulation protocols.

In numerical studies of finite-temperature properties using eigenstate-based method (exact diagonalization or Lanczos calculations), it has for some time been known that the trace over states needed in a quantum mechanical expectation value of some observable A at inverse temperature β ,

$$\langle A(\beta) \rangle = Z_\beta^{-1} \text{Tr}\{Ae^{-\beta H}\}, \quad Z_\beta = \text{Tr}\{e^{-\beta H}\}, \quad (1)$$

does not have to be evaluated completely; it is normally sufficient to average over a small number of states (or even a single state).^{9,10} This observation was made more precise and was utilized as a way to optimize the averaging procedure using “minimally entangled states” in

$T > 0$ calculations with the density-matrix renormalization group method.^{11,12} Here we will show that the concept of typicality can also be used in studies of quantum phase transitions, where the focus is on ground states. Though the target of a calculation in this case is a specific eigenstate, we will show that the typical critical scaling properties also emerge in classes of states that resemble thermal mixed states.

A. Typicality in imaginary time evolution

We work in the context of projector quantum Monte Carlo (PQMC) simulations,^{13,14} where, given an essentially arbitrary initial state $|\Psi_0\rangle$ (often called a “trial state”, though the term is somewhat misleading), the ground state can be found by time evolution in imaginary time,

$$|\Psi(\tau)\rangle = U(\tau)|\Psi(0)\rangle, \quad (2)$$

with $U = \exp(-\tau H)$ and τ sufficiently large in a way that we will make more precise. The expectation of an observable A in the projected state is calculated as

$$\langle A(\tau) \rangle = Z_\tau^{-1} \langle \Psi(\tau) | A | \Psi(\tau) \rangle, \quad Z_\tau = \langle \Psi(\tau) | \Psi(\tau) \rangle. \quad (3)$$

For a finite system of linear size L , the ground state expectation value $\langle 0 | A | 0 \rangle = \langle A(\tau \rightarrow \infty) \rangle$ can always be obtained (provided that $|\Psi\rangle$ has some overlap with it) to arbitrary precision by using some large value of τ . To be systematic, one can, for example, double τ in a series of calculations until the results converge within statistical errors. This is similar to $T > 0$ methods, such as the stochastic series expansion (SSE) quantum Monte Carlo (QMC) method,^{15,16} applied for a series of inverse temperatures $\beta = 1/T$, e.g., $\beta_n = 2^n$, to make sure that the groundstate properties emerge as n is increased (see, e.g.,

Ref. 17 for a case where extremely low temperatures were reached this way).

Although in some cases one would like to reach the true ground state, in studies of continuous quantum critical points it is well known that this is not necessary. Instead, if the dynamic exponent z is known, one can choose $\beta = aL^z$, where z is the dynamic critical exponent, with an arbitrary proportionality factor a . This scaling of β removes the dependence on β from the scaling function, and one can then study finite-size scaling of computed quantities only in the spatial size L . This is often a more practical (less demanding of computer resources) alternative to eliminating the β dependence by effectively taking the limit $\beta \rightarrow \infty$ when studying the true ground state.

In analogy with $T > 0$ simulations of criticality, we will here carry out PQMC calculations with the projection time scaled as $\tau = aL^z$ for a quantum-critical system. This has certainly been done before, under the intuitively clear notion that the temporal boundary conditions should not matter and one can proceed exactly as in $T > 0$ calculations; see, e.g., the recent work in Ref. 18. However, the freedom to choose the trial state is an aspect of the problem not present in $T > 0$ simulations, where one always has periodic imaginary time boundaries. To our knowledge, systematic studies of the role of the trial state and how the typicality emerges irrespective of it and the scale factor in the projection time has not been studied systematically before. We will here demonstrate this independence of the asymptotic scaling behaviors on a as well as the trial state $|\Psi(0)\rangle$, by choosing a range of different trial states and factors. Our results in all cases demonstrate quantum-critical typicality of imaginary-time evolved states. On a practical level, this can save time in PQMC simulations, as the simulation time typically scales linearly with τ and reaching the true ground state to within small error bars may require very large τ and detailed tests to check for convergence. Instead scaling τ as aL with a small factor a can then save significant computer time. However, as one may expect, if a is too small, very large system sizes are required for the asymptotic critical behavior to set in. We will observe how the cross-over depends on a and the trial state and also discuss possible elimination of the leading scaling corrections by identifying an optimal value of a . We will also make other interesting observations on the role of the trial state.

B. Critical Bilayer Heisenberg Model

To validate the above typicality hypothesis, we use the $S = 1/2$ Heisenberg model on a symmetric bilayer,^{19–21} illustrated in Fig. 1, as a concrete example. The Hamiltonian of the model is given by

$$H = J_1 \sum_{\langle i,j \rangle} (\mathbf{S}_{1i} \cdot \mathbf{S}_{1j} + \mathbf{S}_{2i} \cdot \mathbf{S}_{2j}) + J_2 \sum_{i=1}^{L^2} \mathbf{S}_{1i} \cdot \mathbf{S}_{2i}, \quad (4)$$

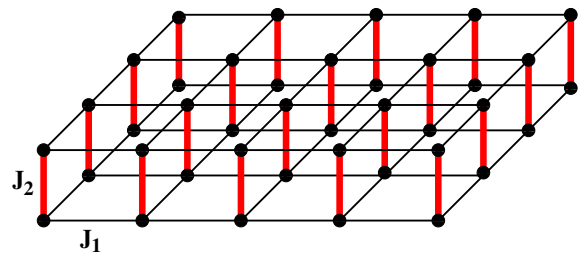


FIG. 1. The bilayer Heisenberg model with two different exchange constants between nearest-neighbor $S = 1/2$ spins; J_1 within the individual layers and J_2 between the layers.

where \mathbf{S}_{ai} is a spin $S = 1/2$ operator at site i of layer $a = 1, 2$ and $\langle i, j \rangle$ denotes a nearest-neighbor pair of spins on the $L \times L$ square lattice. Periodic boundary conditions are applied. The coupling constants J_1 and J_2 are antiferromagnetic (positive). Only even sizes L are considered in our study to avoid frustration due to the periodic boundary conditions imposed.

The bilayer model realizes a quantum phase transition from Néel order for small $g = J_2/J_1$ (e.g., for $g = 0$ the system consists of two decoupled 2D Heisenberg layers, for which the long-range Néel order is well understood and quantified²²) to a quantum paramagnet for large values. For $g \rightarrow \infty$ the ground state is simply a product of singlets on the bond between the layers and there is a spin gap $\Delta = J_2$. This gap closes at g_c , and long-range Néel order forms continuously for $g < g_c$. By symmetry, this $T = 0$ transition in 2+1 dimensions (two space dimensions and one time dimension) should belong to the universality class of the finite-T transition of the three-dimensional (3D) classical Heisenberg model, or O(3) model,^{23–25} provided that the Lorentz invariance is emergent when $L \rightarrow \infty$ (i.e., the dynamic exponent takes the value $z = 1$).

The Néel–paramagnetic transition has been studied intensely, with the bilayer model and several other cases of dimerization; for a review, see Ref. 16. Among the more precise studies of the bilayer, in Ref. 26 SSE calculations were used to determine the critical coupling ratio as $g_c = 2.5220(1)$ (where here and henceforth the number within parenthesis indicates the statistical error of the preceding digit) and the correlation length exponent was found to be $\nu = 0.7106(9)$, which is in agreement with the 3D classical Heisenberg exponent $\nu = 0.7112(5)$ obtained in a high-precision study of the classical 3D ϕ^4 model.²⁷ This exponent is also consistent with that of the 2D columnar dimerized quantum Heisenberg model.²⁸ Initial disagreement with O(3) universality for the case of staggered dimers²⁹ have now been attributed to strong corrections to scaling.^{30–32} Thus, there is little doubt that all these dimerized models belong to the same standard O(3) universality class. Here our goal is not to reconfirm this or to obtain more precise exponents, but to convincingly demonstrate that typicality at the quantum critical fluctuations holds, in the precise sense that the same

O(3) exponents are produced asymptotically (for sufficiently large system size) with different prefactors $a \leq 1$ in the scaling of τ with L in PQMC simulations and with a set of completely different trial states in Eq. (3). We only assume that the dynamical exponent $z = 1$, and extract the other exponents using finite-size scaling of several physical observables.

C. Paper Outline

In Sec. II we review the PQMC method for quantum spin systems in the valence bond (VB) basis, to make clear the role of the boundary conditions of the time evolution. We also introduce the four trial states used in the simulations and define the physical observables and their corresponding PQMC estimators that we use to study the critical fluctuations. In particular, we discuss the estimator of the spin stiffness, which so far has only been derived within $T > 0$ QMC methods but for which we here present a simple generalization for PQMC calculations. In Sec. III we discuss the finite-size scaling ansatz within which we analyze our data. We then determine the critical coupling of the bilayer model and extract its universal exponents at criticality. We also discuss atypical and non-asymptotic properties that originate from the initial trial states and finite projecting time. We summarize the results and further discuss them in Sec. IV.

II. VALENCE-BOND PROJECTOR METHOD

In a PQMC simulation, the ground state $|0\rangle$ of a system is reached by projecting a trial singlet state $|\Psi(0)\rangle$, as described in Eq. (2). For a spin-isotropic, bipartite $S = 1/2$ quantum spin systems, the sampling of Z_τ can be carried in the restricted VB basis,^{13,14,33} where the VBs (singlets) connect sites only on different sublattices. The arbitrary trial singlet state $|\Psi(0)\rangle$ is expressed in the VB basis as

$$|\Psi(0)\rangle = \sum_r w_r |V_r\rangle, \quad (5)$$

where $|V_r\rangle$ is a tiling of $N/2$ singlets $(a, b) = \uparrow_a \downarrow_b - \uparrow_b \downarrow_a$ on a lattice with N sites, with a and b referring to sites on sublattice A and B, respectively, and the coefficients w_r are all positive. These conventions correspond to Marshall's sign rule for the ground state of a bipartite systems.

A. Sampling space

An antiferromagnetic Heisenberg Hamiltonian can be written as a sum $-\sum_{ij} J_{ij} P_{ij}$ of singlet projectors,

$$P_{ij} = 1/4 - \mathbf{S}_i \cdot \mathbf{S}_j. \quad (6)$$

When projecting with a high power $(-H)^n$ of the Hamiltonian, a PQMC configuration corresponds to a string of

n of these singlet projectors acting on a component (a singlet tiling) of the VB trial state. Instead of the fixed power, one can also, as we will do here, use the Taylor expansion of $e^{-\tau H}$ and sample strings of a fluctuating number n of operators. When a singlet projector acts on a VB state, either the two sites ij are connected by the same bond, in which case the state stays unchanged, or the sites belong to two different bonds that become reconfigured so that one of the new bonds connects sites i and j and the second one connects the two sites that were previously connected to i and j . The latter process comes with a factor $1/2$ in the weight of a configuration, while the factor is unity in the former case. One can formulate a PQMC algorithm based on these simple rules purely in the VB basis,¹⁴ but the sampling is rather slow compared to state-of-the art $T > 0$ methods.

By sampling the spin configurations corresponding to a given singlet tiling of the trial state, one can formulate a PQMC algorithm that is very similar to the $T > 0$ SSE method running at $\beta = 2\tau$, including very efficient loop updates.³⁴ Let us compare the two approaches. In the SSE method, $e^{-\beta H}$ is Taylor expanded up to all contributing orders n , with the maximum contributions of order $n = -\beta \langle H \rangle \propto \beta N$. The expansion order n is sampled in the simulation according to the total weight of contributions from that order. Often, for practical reasons, a self-selected upper bound n_{\max} is imposed, so that the sampling scheme can be formulated with a fixed number of operators in the operator strings corresponding to the evolution of traced-over states $|\alpha\rangle$ in the chosen basis (normally the basis of S_i^z spins). Then n of these n_{\max} operators are selected among the terms H_b of the Hamiltonian and the remaining $n_{\max} - n$ entries are “fill-in” identity operators.

Essentially, going from the SSE to the PQMC method corresponds to opening up the periodic time boundaries arising from the trace operation, formally replacing the trace $\sum_\alpha \langle \alpha | \cdots | \alpha \rangle$ by a sum $\sum_{\alpha_L, \alpha_R} c_L c_R \langle \alpha_L | \cdots | \alpha_R \rangle$ corresponding the projection out of the trial state. In the valence bond basis, this results in “sealing” open loop segments at the time boundaries with VBs. Then, as in the SSE case, a space-time spin configuration can be fully decomposed into loops that can be flipped independently of each other. One can show that all signs cancel out in the overall weights for the PQMC configurations, because of the bipartiteness of the system.

The spin and valence bond representations of a configuration are illustrated by an example in Fig. 2, including the concept of loop updates in the spin representation, Fig. 2(a). The VBs in the trial state can be updated by simple reconfigurations of pairs of bonds, to maintain the A-B connectivity with anti-parallel spins on each bond, using the weights w_r in standard Metropolis acceptance probability. One can also formulate loop updates of the trial state,³⁴ but this is more useful in variational calculations than in PQMC.

When evaluating operator expectation values, it is normally (depending on the type of operator considered)

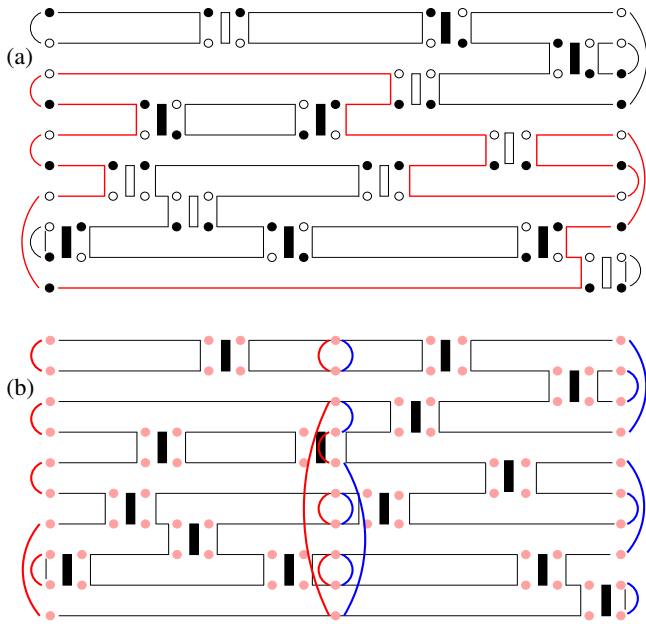


FIG. 2. Two different representations used for the configuration space in PQMC simulation in the VB basis, exemplified with a Heisenberg chain of 10 sites. VBs of the sampled trial state are shown at the left and right edges. In (a), the linked vertex representation used for loop updates is shown, with solid and open circles indicating up and down spins. Diagonal and off-diagonal operators, $-(S_i^z S_j^z - 1/4)$ and $-(S_i^+ S_j^- + S_i^- S_j^+)$ are denoted by open and solid vertical bars, respectively. An example of a loop is shown in red; flipping this loop changes all up spins to down, and vice versa, thereby also changing the operator type (diagonal or off-diagonal) on some of the vertices. The number of operators n and their locations on the lattice are updated separately in “diagonal updates”. In (b), the pure VB representation used for collecting operator expectation values is shown for the same configuration. Here there is no distinction between diagonal and off diagonal operators and the bars indicate the full singlet projectors P_{ij} . Propagated left and right VB configurations are shown at the center; they make up the transition graph on which correlation functions are evaluated.

better to return to the VB only basis, illustrated in Fig. 2(b), which corresponds to summing over all spin configurations that are compatible with the VBs in the trial state and the lattice locations of the operators in the string—here also all the operators turn into the full singlet projectors P_{ij} , instead of their individual diagonal and off-diagonal terms in the spin basis.

In principle, we do not have to sample VBs of the trial state; we can just use a fixed configuration of the VBs and that will still have overlap with the ground state and converge to the same. However, one can also construct good, practically workable variational states and this can improve the convergence properties.³⁴ Even without optimizing, one can write down simple translationally invariant states to further restrict the simulations to total momentum $k = 0$. In $T > 0$ simulations, states with all \mathbf{k} and all total spin values S are included, and to reach

the ground state T has to be well below the smallest gap from the $k = 0, S = 0$ ground state. PQMC simulations are restricted by construction to $S = 0$ and $k = 0$, and, thus, most of the low-energy states are excluded from the outset and do not have to be projected away. Here our purpose is not to reach the ground state perfectly, and we will test the typicality hypothesis both with $k = 0$ trial states and with simple “frozen” VB states that do not conserve \mathbf{k} .

B. Different Trial States

The amplitude-product states proposed by Liang *et al.*^{13,33} are good $k = 0$ variational states to describe Néel ordered, critical, and quantum paramagnetic systems. The wave-function coefficients are of the form

$$w_r = \prod_{i=1}^{N/2} h(\mathbf{r}_i), \quad (7)$$

where \mathbf{r}_i denotes the “shape” of the i -th singlet (the lengths of the VB in all lattice directions) and $h(\mathbf{r}_i) > 0$ should respect all lattice symmetries of a translationally invariant system. A commonly used form is $h(\mathbf{r}) = |\mathbf{r}|^{-\alpha}$ with $|\mathbf{r}|$ the length of the VB and $\alpha > 0$ an exponent that can be optimized; for example, for the 2D Heisenberg model the best choice is $\alpha = 3$.³⁵ Variational optimization of the amplitudes can give extremely good energies—probably the best variational energies ever achieved for Heisenberg models.^{36,37} Here again we primarily want to compare different trial states, and we define $|\Psi_1\rangle$ with $\alpha = 3$ and $|\Psi_2\rangle$ with $\alpha = 6$.

As the third trial state we choose a single VB configuration,

$$|\Psi_3\rangle = \prod_{i=1}^{L^2} (i_1, i_2), \quad (8)$$

which is a product state of singlets (i_1, i_2) on the vertical bonds connecting two adjacent sites i_1 and i_2 in different layers. It is the asymptotic ground state of the Hamiltonian (4) in the limit $J_2 \rightarrow \infty$; thus the time evolution can be understood as an imaginary-time quench in the couplings of the system from $g = \infty$ to g close to g_c (when studying criticality), followed by a waiting time τ .

The last trial state is again a simple VB configuration, but, unlike $|\Psi_3\rangle$, it breaks the translational symmetry of the system. We choose a columnar arrangement of the VBs in each layer;

$$|\Psi_4\rangle = \prod_{a=1,2} \prod_{x'_{ai}} (i_a, i_a + \hat{x}), \quad (9)$$

where $i_a + \hat{x}$ stands for the site shifted from i_a by one lattice spacing along the x direction and x'_{ai} denotes a site i of layer a whose x coordinate is odd.

The energy expectation values $E = \langle H \rangle / N$ of the above trial states can be evaluated by sampling the VBs of $|\Psi_1\rangle$ and $|\Psi_2\rangle$, and for $|\Psi_3\rangle$ and $|\Psi_4\rangle$ exact calculations are trivial. For $L = 16$, as an example, the results at the estimated critical point $g = 2.5222$ (see further below) are $E_1 = -1.841(1)$, $E_2 = -1.829(1)$, $E_3 = -1.7611$, and $E_4 = -1.190275$. The unbiased, sufficiently projected energy is $E = -1.94225(2)$. Obviously, the last two trial states are far away from good variational states describing the criticality of the current model. Even $|\Psi_1\rangle$ and $|\Psi_2\rangle$ are not very good variational states, and much better ones can in principle be obtained by optimizing the bond amplitudes. However, our purpose here is not to optimize the states and the simulations, but to demonstrate that typical critical fluctuations emerge out of arbitrary trial states with projection time $\tau \propto L$. For this purpose the above range of trial states will suffice.

C. Physical Observables and PQMC Estimators

The staggered magnetization, the order parameter, is defined as

$$\mathbf{m} = \frac{1}{N} \sum_{i=1}^N (-1)^{x_i+y_i+z_i} \mathbf{S}_i, \quad (10)$$

where (x_i, y_i, z_i) are the integer coordinates of the spin at site i of the bilayer with $N = 2L^2$ sites. The squared magnetization $\langle \mathbf{m}^2 \rangle$ can be efficiently estimated in PQMC simulations using the sum of squared loop lengths in the transition graph obtained by superimposing the sampled “left” and “right” projected VB configurations,³⁹ as illustrated in Fig. 2(b).

The Binder ratio⁴⁰ is defined as

$$Q = \frac{\langle \mathbf{m}^4 \rangle}{\langle \mathbf{m}^2 \rangle^2}, \quad (11)$$

where \mathbf{m}^4 can also be calculated according to the loop structure of the transposition graphs.³⁹

The spin stiffness ρ_s characterizes the tendency of ordered spins to adapt in response to a twist imposed on the spins in an ordered state in a direction perpendicular to the ordering vector. In the common QMC simulations at finite temperature, e.g., with the SSE method¹⁶ or path integrals,⁴¹ there is a very convenient estimator based on fluctuations of the winding number characterizing the topology of the spin world lines propagated around the space-time periodic system. The stiffness along the α lattice direction is given by

$$\rho_s = \frac{\langle W_\alpha^2 \rangle}{L^{d-2} \beta}, \quad (12)$$

with the size normalized winding number defined in the SSE method as

$$W_\alpha = \frac{1}{L} (N_\alpha^+ - N_\alpha^-). \quad (13)$$

Here N_α^+ and N_α^- denote the total number of off-diagonal operators transporting spin in the positive and negative α direction, respectively. So far, the spin stiffness has not been considered in PQMC simulations, as far as we are aware, likely because the winding number is not a well defined conserved topological number in this case. However, it is still possible to proceed with an unbiased generalization of the above winding number estimator, as we describe next.

The winding number formula (13) is a consequence of the periodic boundaries in both the spatial and time directions at $T > 0$. The “cutting open” of the time boundaries in the PQMC method makes this estimator fail at first sight. However, since the current fluctuations within some local time segment $\Delta\tau$ should be independent of β for large β , and these fluctuations are what gives rise to the winding numbers, it is clear that the conservation of the winding number is not very consequential in Eqs. (12) and (13), but is just a byproduct of the periodic time boundaries in combination with the conserved magnetization of the system. Thus, it should be possible to generalize the formula by considering generalized, non-integer winding numbers over a sufficiently large time interval $\Delta\tau \leq 2\tau$, where we recall that the total length of the system in imaginary time is 2τ . Since the time dimension is not uniform, due to the open boundaries, one can also presume that convergence to the correct value when $2\tau, \Delta\tau \rightarrow \infty$ will be faster if $\Delta\tau < 2\tau$ and the interval is time-centered.

As a reasonable choice satisfying the above requirements, we take the centered interval with $\Delta\tau = \tau$ and calculate the spin stiffness of a d -dimensional system according to

$$\rho_s = \frac{\langle (\tilde{N}_\alpha^+ - \tilde{N}_\alpha^-)^2 \rangle}{\tau L^d} \quad (14)$$

where \tilde{N}_α^+ and \tilde{N}_α^- denote the total number of operators transporting spin in the positive and negative α direction by the middle part of the operator string. We have used the fact that the total length is linearly proportion to 2τ , which is β in a corresponding SSE simulation.

To validate the above formula, we simulate the square lattice Heisenberg model with system size $L = 16$ using both the SSE and PQMC methods. Results obtained by the two methods are shown versus β and 2τ in Fig. 3). As the ground state is approached for large β and τ , we can see convergence to the same value. We find $\rho_s = 0.13239(2)$ from winding number fluctuations in the SSE simulations and $0.1324(1)$ from the generalized spin current definition in Eq. (14) in the PQMC simulations. The two estimates agree perfectly. In the case of SSE, we expect asymptotic exponentially fast convergence (though the above result was obtained by extrapolation using a polynomial, which should be fine at the level of the statistical error bars), reflecting the finite-size gap in the spectrum, while in the case of the PQMC calculations with the estimator (14) the convergence appears to be linear in $1/\tau$. We do not currently have an

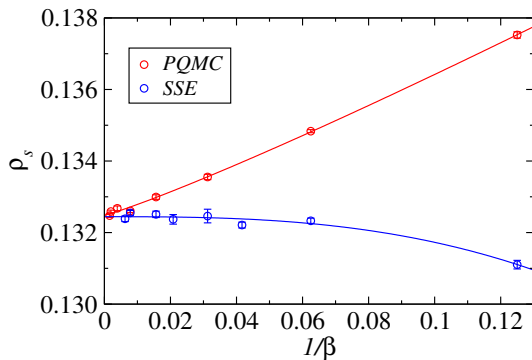


FIG. 3. Spin stiffness of the 2D Heisenberg model on the square lattice of linear size $L = 16$ as a function of inverse temperature β in SSE simulations or the projection time $2\tau = \beta$ in PQMC simulations. The results were obtained using the standard winding number fluctuations according to Eq. (12) and the corresponding generalized spin current formula (14), in the SSE and PQMC simulations, respectively.

understanding of this behavior, though clearly it must be related to the fact that the $\Delta\tau$ region over which the current fluctuations are summed have open boundaries and one may expect a correction proportional to the inverse of the length of the boundary. Thus, SSE may still be the preferable way to compute ρ_s , though certainly this test (and others) shows that this important physical quantity can also be reliably obtained in PQMC calculations.

III. CRITICAL PROPERTIES

A. Finite-size Scaling Ansatz

For a singular quantity $A \propto \delta^\kappa$ in the thermodynamic limit, according to the standard finite-size scaling theory,⁴² scaling of the following form is expected close to the critical point g_c :

$$A(g, L) = L^{-\kappa/\nu} f(\delta L^{1/\nu}, L^{-\omega}), \quad (15)$$

where $\delta = (g - g_c)/g_c$, the exponent κ depends on the quantity in question, and both κ and ν are tied to the universality class of the transition. We have included only the most important scaling correction, with the associated exponent $\omega > 0$. Exactly at g_c ($\delta = 0$), and neglecting the scaling correction for now, the form reduces to

$$A(g_c, L) \propto L^{-\kappa/\nu}, \quad (16)$$

given that the non-singular scaling function f approaches a constant when $\delta \rightarrow 0$.

To locate the critical point, we can treat the scaled $A(g, L)L^{\kappa/\nu}$ as a dimensionless quantity $\tilde{A}(g, L)$. By Taylor expanding the scaling function in (15) and keeping the correction, we have

$$\tilde{A}(g, L) = \tilde{A}_c + a_1 \delta L^{\frac{1}{\nu}} + a_2 \delta^2 L^{\frac{2}{\nu}} + b_1 L^{-\omega} + c_1 \delta L^{\frac{1}{\nu} - \omega} + \dots \quad (17)$$

where $\tilde{A}_c, a_1, a_2, b_1, c_1$ are unknown, non-universal constants. This implies that curves $\tilde{A}(g, L_1)$ and $\tilde{A}(g, L_2)$ versus g cross each other at some $g = g^*(L_1, L_2)$. We will take $L_1 = L$ and $L_2 = 2L$, for which the crossing point $g^*(L)$ approaches g_c as⁴³

$$g^*(L) - g_c \propto L^{-(1/\nu + \omega)}. \quad (18)$$

The critical point g_c can thus be extrapolated. The critical value of \tilde{A}_c may also be universal and is therefore interesting. It can be extracted by calculating the quantity $\tilde{A}^*(L) \equiv \tilde{A}(g^*, L)$ at the crossing point $g^*(L)$, which approaches its limit \tilde{A}_c in the following way

$$\tilde{A}^*(L) - \tilde{A}_c \propto L^{-\omega}. \quad (19)$$

In principle both ω and ν can be extracted from Eqs. (18) and (19), though in practice the neglected higher-order corrections often distort the values significantly. One can instead extract $1/\nu$ from the slope of $\tilde{A}^*(L)$ at the crossing point, as described in many papers (including a recent systematic study in the Supplemental Material of Ref.⁴⁴).

Alternatively the correlation exponent ν can also be estimated by staying at the size-extrapolated critical point, if this point has been located to sufficient precision. We will use this approach here. First, we calculate the derivative $s(g_c, L)$ of \tilde{A} to g at the estimated critical point g_c . This is done by fitting a polynomial $f(g) = ag^2 + bg + c$, with three unknown constants a, b, c , to six values of $\tilde{A}(g, L)$ near g_c . Error bars can be estimated by Gaussian noise propagation. Then, according to the following scaling formula,

$$s(g_c, L) = \left. \frac{d\tilde{A}(g, L)}{dg} \right|_{g_c} = a_1 L^{\frac{1}{\nu}} (1 + bL^{-\omega}), \quad (20)$$

we find ν by using nonlinear fits to the slopes. We will here exclude small system sizes so that the correction can be safely neglected, given that the correction exponent is relatively large; $\omega \approx 0.78$.²⁷

The Binder ratio Q is dimensionless, which means $\kappa = 0$, while for the spin stiffness ρ_s , $\kappa = (d + z - 2)\nu$, or $\kappa = \nu$ in the present case where $d = 2, z = 1$.⁴⁵ Therefore Q and $\rho_s L$ are useful observables for locating the critical point and estimating the correlation exponent ν .

For the order parameter \mathbf{m} , κ is the exponent β , which leads to the scaling behavior of the squared staggered magnetization,

$$\langle \mathbf{m}^2 \rangle \propto L^{-2\beta/\nu} (1 + cL^{-\omega}), \quad (21)$$

at the critical point, with c a constant. According to the scaling relation $2\beta/\nu = 1 + \eta$, we can estimate η from the size dependence, where, again, we typically do not include the correction term.

B. The Critical Point

We next study the typical behavior of the critical fluctuations, by performing PQMC simulations of the bilayer

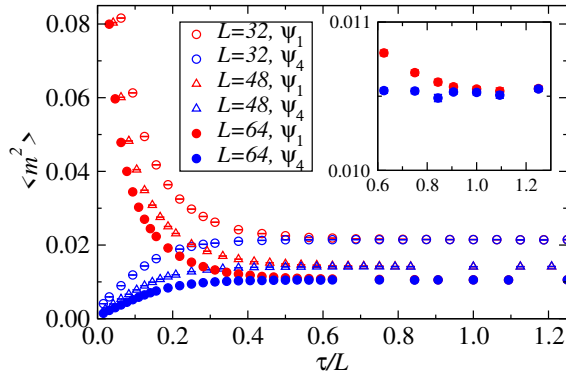


FIG. 4. The squared sublattice magnetization obtained in critical bilayer PQMC simulations with system sizes $L = 32, 44$, and 64 , with the trial states $|\Psi_1\rangle$ and $|\Psi_4\rangle$ (representing the best and worst state as judged by the variational energy). The inset shows the $L = 64$ results close to $\tau = L$ on a more detailed scale.

Heisenberg model with the four different trial states defined above and with different prefactors a in $\tau = aL$ and using L up to 128 . We typically used 10^5 MC steps to equilibrate the system and 10^6 for collecting data for the physical quantities of interest. To project out the ground state fully, τ needs to satisfy $\tau \gg 1/\Delta$, with Δ the gap between the ground state and the first excited state “seen” in the calculations, which in the VB basis is the second singlet state. If we can find good scaling properties even significantly away from this limit, it means that a band of low-lying singlets also share the same critical fluctuations as the ground state.

In Fig. 4, we first show results for the squared order parameter evaluated at the critical point, estimated below to be $g_c \approx 2.5222$, as a function of the projection time for three system sizes and two trial states. On the scale used in the figure, $\tau = L$ gives results almost indistinguishable from the ground state—a close examination (inset of the figure) reveals that there are still some statistically significant differences. With the worst of the trial states $|\Psi_4\rangle$, the results have visibly not converged for $\tau = L/2$, and at $\tau = L/4$ and smaller both trial states give results clearly different from the ground state. Note that one $|\Psi_1\rangle$ has strong Néel that is decays away with increasing τ , while $|\Psi_4\rangle$ has no long-range correlations at all; thus the critical correlations are gradually emergent with increasing τ . Thus, we have a range of different trial states and it is interesting to see if the critical correlations can emerge universally even for small factors a in $\tau = aL$, where the behaviors in Fig. 4 look completely different for the two trial states.

To analyze the critical point, we begin by considering the time regime where we have almost reached the ground state, using the best trial state in the variational sense, $|\Psi_1\rangle$, and the projection time set to $\tau = L$, i.e., the factor $a = 1$. The scaled spin stiffness $\rho_s L$ and the Binder ratio Q are shown versus the coupling ratio g for various system sizes in Fig. 5. The results do not differ appreciably

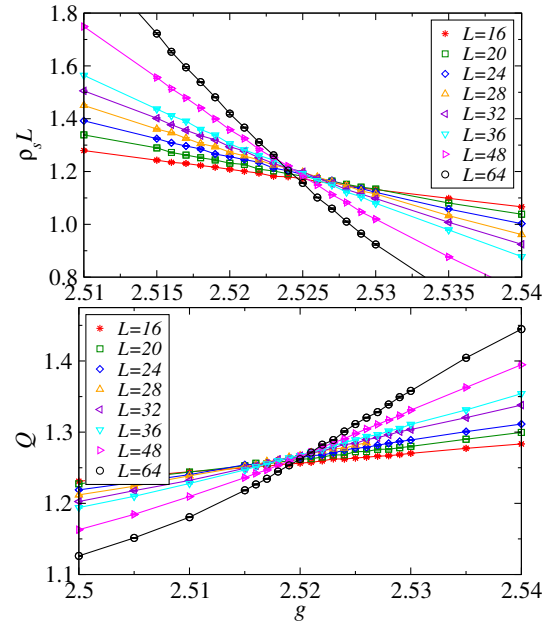


FIG. 5. The scaled spin stiffness $\rho_s L$ (a) and the Binder ratio Q (b) of the bilayer Heisenberg model with several L graphed vs the coupling ratio g . The PQMC calculations were carried out using $\tau = L$ ($a = 1$).

from SSE results obtained at very low temperatures,²⁶ indicating that the projection time here brings us almost to the ground state. We find crossing points between results for system sizes L and $2L$ using polynomials fitted to the data points. These crossing points extracted for the two different quantities for a large number of size pairs are shown in Fig. 6(a). The drifts of the g^* values obtained from both quantities are monotonic in L , and both of them converge to a common critical point g_c rapidly for large L . All $L \geq 16$ points are consistent with the expected power-law, Eq. (18).

A nonlinear fit of $g^*(L)$ from the $\rho_s L$ crossings yields $g_c = 2.52222(4)$ and $1/\nu + \omega = 1.65(3)$, with a reasonable reduced goodness-of-fit value $\chi^2 = 1.2$. Here the result for the exponent combination $1/\nu + \omega$ is not very close to the expected $O(3)$ value, $1/\nu + \omega \approx 2.2$, likely reflecting the role of remaining higher-order corrections. Such still not size-converged “effective exponents” are known to not significantly effect the extrapolated critical point value.⁴⁴ A similar fit of g^* of Q gives $g_c = 2.52224(6)$ and $1/\nu + \omega = 2.3(1)$, with reduced $\chi^2 = 1.6$. Both estimates of critical point agree well with earlier estimate $g_c = 2.5220(1)$ obtained by using SSE QMC²⁶, in which the ground-state properties were obtained by the β doubling approach, but the statistical error is significantly reduced.

We next consider results obtained with the other trial states: $|\Psi_2\rangle$, $|\Psi_3\rangle$, and $|\Psi_4\rangle$. The projection lengths are first all set as $\tau = L$. The $(L, 2L)$ crossing points g^* from $\rho_s L$ and Q are both shown in Fig. 6(a) together with the previous results based on $|\Psi_1\rangle$. We see only small

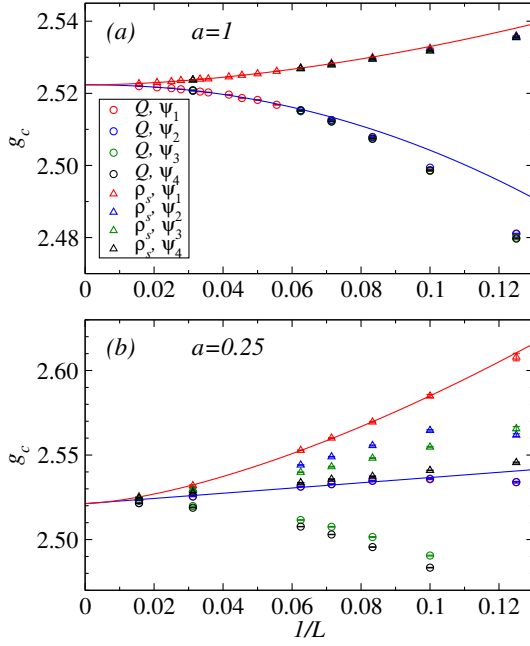


FIG. 6. Scaling of crossing points $g^*(L)$ of the size-scaled spin stiffness $\rho_s L$ (triangles) and the Binder ratio Q (circles). The results were obtained from four different trial states, as indicated by the legends, and two different projection time factors a were in the PQMC simulations; $a = 1$ in (a) and $a = 0.25$ in (b). The largest system size pair is $(L, 2L) = (64, 128)$. The solid curves are fits to g^* from $\rho_s L$ crossings (red) and Q (blue) obtained from states projected out of the best trial state, $|\Psi_1\rangle$.

differences between the results from the different trial states and, not surprisingly, all these crossings converge to the common critical coupling g_c . Though it is not apparent from the figure, somewhat larger system sizes are needed to fit the $|\Psi_{t>1}\rangle$ results to power-law forms than what is the case with $|\Psi_1\rangle$. The latter state also is the best state in the sense of the variational energy. The results of all the fits are listed in Tab. I, including the smallest size used in the fit.

Since the above $a = 1$ simulations deliver results quite close to the ground state for all the trial states, we need to go to smaller a to investigate the emergence of critical typicality in greater detail. Crossing points obtained from the $\tau = L/4$ simulations are shown in Fig. 6(b). Here we can see very significant differences from the $\tau = 1$ data, but all crossing points still flow toward the same critical point. Results of extrapolations are summarised in Tab. I.

C. Critical Exponents

We next validate that the states projected out from various trial states at $\tau \propto L$ display typical critical fluctuations characterized by the correct critical O(3) exponents. We demonstrate that this universality emerges

with increasing system size in finite-size scaling for all the different trial states.

First, we show that the correlation exponent ν can be extracted from the projected states. We extract the exponent according to Eq. (20) from the g derivatives $s(g, L)$ of the curves $Q(g)$ at the estimated critical point, $g_c = 2.5222$. The derivatives are extracted from a quadratic polynomial fitted to a set of points for g in the neighborhood of g_c . Results are shown in Fig. 7.

In the case $a = 1$, for all four trial states and for data from both $\rho_s L$ and Q , the derivatives reproduce the expected power-law behavior (20) as shown in Fig. 7(a). Here we do not include the correction term $L^{-\omega}$, where $\omega \approx 0.78$ is expected for the universality class, as we find that the prefactor is small and good fits to just the leading power law $L^{1/\nu}$ can be achieved if some of the smaller systems are excluded. Thus, we extract the correlation exponent ν from the data for each trial state by fitting to Eq. (20), starting from system sizes L_{\min} sufficiently large for the quality of the fit to be acceptable. To avoid the systematic error induced by the small deviations of our g_c value from the true critical point, we here only use system sizes up to $L = 64$. We have estimated that the deviations will then affect the extracted exponents less than the purely statistical errors of the fitting parameters. All estimated ν values for the four trial states are consistent with each other and with the known value of the exponent. The results are listed in Tab. II. We can see good agreement with the correct O(3) exponent in all cases.

For $a = 0.5$, the data, shown in Fig. 7(b), show more dependence on the trial state, but in all cases the slope takes the expected value for sufficiently large system sizes. For $a = 0.125$, we can see very significant depen-

TABLE I. Results of finite-size analysis with a single power-law correction to the critical point g_c for different trial states and different value of the projection factor a . The standard goodness-of-fit per degree of freedom is denoted as χ^2 .

trial state	$a = 1$					
	$g_c(\rho_s)$	$\chi^2(\rho_s)$	L_{\min}	$g_c(Q)$	$\chi^2(Q)$	L_{\min}
Ψ_1	2.52222(4)	1.2	8	2.52224(6)	1.6	16
Ψ_2	2.5221(1)	0.5	12	2.5220(4)	0.6	12
Ψ_3	2.5220(2)	1.0	12	2.5219(4)	1.2	12
Ψ_4	2.5220(8)	0.5	12	2.5218(5)	0.6	12
	$a = 0.5$					
	$g_c(\rho_s)$	$\chi^2(\rho_s)$		$g_c(Q)$	$\chi^2(Q)$	
Ψ_1	2.5215(4)	0.3	12	2.5221(1)	0.7	12
Ψ_2	2.5218(3)	1.9	12	2.5221(4)	0.8	12
Ψ_3	2.5220(2)	0.6	12	2.5221(1)	1.1	12
Ψ_4	2.5220(2)	0.6	12	2.5221(2)	1.5	12
	$a = 0.25$					
	$g_c(\rho_s)$	$\chi^2(\rho_s)$		$g_c(Q)$	$\chi^2(Q)$	
Ψ_1	2.5213(2)	0.9	12	2.5213(4)	1.7	12
Ψ_2	2.5222(2)	0.8	12	2.5222(1)	1.4	12
Ψ_3	2.5220(8)	1.4	12	2.5223(3)	0.4	12
Ψ_4	2.5224(5)	2.3	12	2.5212(3)	1.4	12

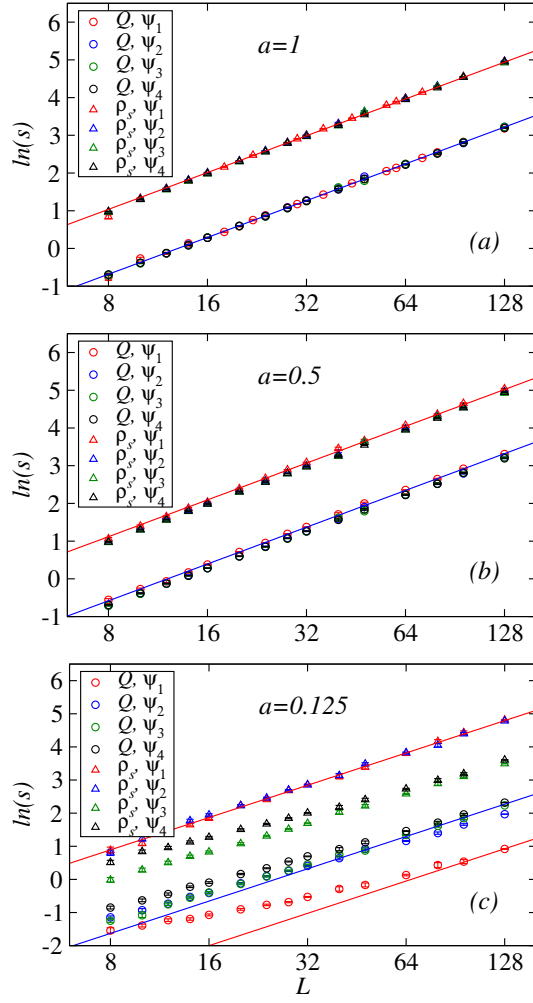


FIG. 7. The derivatives with respect to g of $\rho_s L$ (triangles) and Q (circles) at the best estimated critical point $g_c = 2.5222$, graphed versus the system size on logarithmic scales. Three different projection times $\tau = aL$ were used; (a) $a = 1$, (b) $a = 0.5$, (c) $a = 0.125$. Different graphing colors refer to results obtained with different trial states. The solid lines with slope corresponding to the known value of the exponent, $\nu = 0.7112$, in Eq. (20) are drawn to show the expected large- L behavior.

dence on the trial state, but here as well the slope eventually crosses over to the correct critical form for large L . The results for $a = 0.5$ are also listed in Tab. II, but for $a = 0.125$ we did not carry out the analysis in detail because of the small number of points falling in the asymptotic scaling regime. Nevertheless, these tests make clear that there is a cross-over size, which increases with decreasing a and depends on the trial state, above which the critical $O(3)$ scaling is obtained. The non-universal prefactor of the scaling function depends strongly on a and the trial state.

Next, we investigate the exponent η (the anomalous dimension) of the critical correlation function. We use the squared staggered magnetization $\langle \mathbf{m}^2 \rangle$ at $g_c = 2.5222$.

In this case we include all our large system sizes in the fits, based on an estimation of the effects of the precision of the g_c values. For $a = 1$, as shown in Fig. 8(a), the square order parameter $\langle \mathbf{m}^2 \rangle$ scales well according to the expected critical form Eq. (21) with increasing size L , with only a very weak dependence on the trial state. For the case $a = 0.25$, significant differences in the values of $\langle \mathbf{m}^2 \rangle$ can be observed for the different trial states, as illustrated in Fig. 8(b). Nevertheless, each group of data points from the same trial state forms a straight line on the double-log graph. For large enough L the correction to scaling vanishes and within statistical errors the slopes of the four lines are identical and fully consistent with the known value of η . Fitting to the expected finite-size form, again leaving out system sizes smaller than L_{\min} chosen such that the fits are acceptable, we obtain values listed in Tab. III for $a = 1$ and 0.5 . For $a = 0.25$, the results are also consistent with the $O(3)$ exponent, but the statistical errors are much larger, due to the large L_{\min} needed in this case, and we do not list the results.

D. Critical Binder Ratio

We have shown that typical critical fluctuations emerge out of arbitrary trial states when projecting in imaginary time $\tau \propto L^z$, instead of projecting fully to the ground state of each finite system. However, as mentioned, from the point of view of the path integral picture of the PQMC simulations, we can understand a as time-space aspect ratio, with the initial trial states corresponding to different kinds of boundary conditions. One can also think of this as a sudden quench, where the Hamiltonian is changed at $\tau = 0$ from the one (some times unknown one) for which the trial state is the ground state to the critical Hamiltonian, followed by time evolution with the latter.

While the critical exponents are independent of the

TABLE II. Exponent ν obtained from the g derivatives of $\rho_s L$ and Q at the best estimated critical point g_c . To minimize the systematic errors originating from the deviation of the g value used from the true critical point, we only used system sizes up to $L = 64$ in the fits giving the results shown here. The minimum size is indicated in each case.

a=1						
trial state	$\nu(\rho_s)$	$\chi^2(\rho_s)$	L_{\min}	$\nu(Q)$	$\chi^2(Q)$	L_{\min}
Ψ_1	0.705(7)	1.3	24	0.716(7)	1.5	16
Ψ_2	0.706(5)	1.4	24	0.718(7)	1.3	24
Ψ_3	0.707(7)	1.5	24	0.710(6)	1.1	16
Ψ_4	0.713(7)	1.3	28	0.711(5)	0.9	16
a=0.5						
	$\nu(\rho_s)$	$\chi^2(\rho_s)$	L_{\min}	$\nu(Q)$	$\chi^2(Q)$	L_{\min}
Ψ_1	0.704(20)	1.5	32	0.709(20)	0.9	28
Ψ_2	0.709(8)	0.9	20	0.709(8)	1.4	12
Ψ_3	0.707(9)	0.8	28	0.714(9)	0.8	24
Ψ_4	0.709(10)	1.3	24	0.708(9)	1.1	16

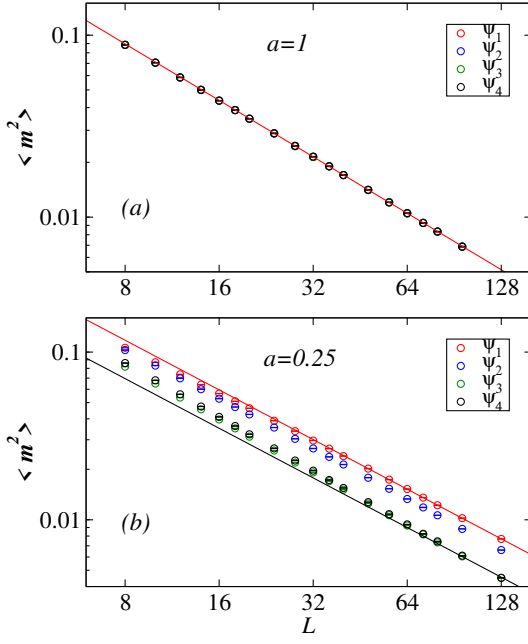


FIG. 8. The squared order parameter at the best estimated critical point $g_c = 2.5222$ versus the system size. for (a) $a = 1$ and (b) $a = 0.5$. The solid lines are fits to the large- L data.

system geometry, the critical value of the Binder ratio Q is universal only in the sense that the value is determined by the dimensionality and symmetry of the system, irrespective of the details of interaction and lattice structure, but under the condition that the boundary conditions and the geometry, e.g., aspect ratio is fixed.^{46,47} This implies that changing the temporal boundary conditions and the aspect ratio should affect the critical value of Q . Therefore it is expected that the critical value of Q in the current PQMC simulations will change with different trial states and factor a in the time scaling $\tau = aL$. We investigate this dependence next

Figure 9(a) shows the Binder ratio at $g_c = 2.5222$ versus $1/L$ in simulations with the four different trial states and two aspect ratios. It is clearly seen that Q_c changes dramatically when a changes from 1 to 0.125 for each of

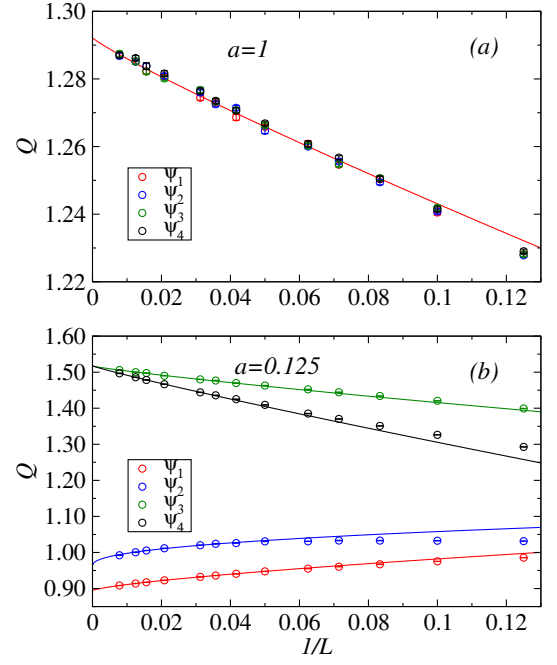


FIG. 9. Critical Binder ratios obtained in simulations with various trial states after projection time $\tau = aL$ with (a) $a = 1$ and (b) $a = 0.125$. The four curves are power-law fits used to extract the infinite-size values. In (a) we only show the fit to data from trial state $|\Psi_1\rangle$, for the sake of clarity.

the trial states. The value of Q_c can be found by fitting Eq. (19) to the data. However, for $a = 1$, the results for Q_c obtained with all trial states seem to converge to the same value when $L \rightarrow \infty$; for $|\Psi_1\rangle$, $Q_c = 1.290(3)$, with reduced $\chi^2 = 0.9$ and starting size $L_{\min} = 32$; for $|\Psi_2\rangle$, $Q_c = 1.289(2)$ ($\chi^2 = 1.1$, $L_{\min} = 20$), for $|\Psi_3\rangle$, $Q_c = 1.291(3)$ ($\chi^2 = 1.1$, $L_{\min} = 20$); for $|\Psi_4\rangle$, $Q_c = 1.289(2)$ ($\chi^2 = 0.5$, $L_{\min} = 32$). In these fits, the exponent ω in all cases is consistent with the known value $\omega \approx 0.78$, though with relative statistical errors of about 20% typically. The extrapolated values of Q agree well with $Q_c \approx 1.293(3)$ previously obtained for an “incomplete bilayer” Heisenberg model (where the intra-layer couplings are missing on one layer), but differs slightly from the result for the complete bilayer Heisenberg model, $Q_c = 1.2858(3)$;²⁶ most likely this disagreement is due to an underestimated error bar in the previous calculation.

In the case of small $a = 0.125$, it is clearly seen in Fig. 9(b) that the differences in Q_c obtained with different trial state can be drastic. Nevertheless, $Q_c = 1.519(3)$ from $|\Psi_3\rangle$ and $Q_c = 1.523(4)$ from $|\Psi_4\rangle$ are still very similar; perhaps even identical asymptotically. (The exponent ω found in the two fits agree well with 0.78.) This may seem surprising, since these trial states are quite different and have different variational energies. The trial states are similar in the sense that they are simple product states of singlets on neighboring sites, but in one case the translational symmetry is broken and in one

TABLE III. Exponent η obtained from finite-size scaling of the staggered magnetization $\langle m^2 \rangle$ at the estimated critical point g_c , using the different trial states and projection times. The O(3) value of the exponent is $\eta = 0.0375(5)$.²⁷

a=1				
trial state	Ψ_1	Ψ_2	Ψ_3	Ψ_4
η	0.036(3)	0.032(3)	0.038(6)	0.039(3)
χ^2	1.6	1.6	1.8	1.3
L_{\min}	48	24	18	40
a=0.5				
trial state	Ψ_1	Ψ_2	Ψ_3	Ψ_4
η	0.026(6)	0.036(1)	0.037(2)	0.036(4)
χ^2	1.9	1.6	1.9	0.81
L_{\min}	16	20	20	56

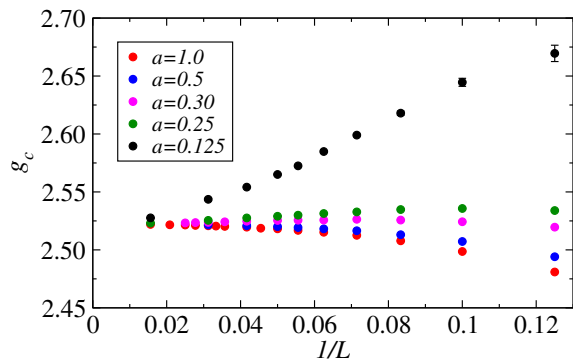


FIG. 10. Crossing point between Binder cumulants for system sizes $(L, 2L)$ graphed versus $1/L$ for different time scalings $\tau = aL$ with the trial state $|\Psi_1\rangle$.

case it is not. One may speculate that the value of the Binder ratio for small a and $L \rightarrow \infty$ is related to the entanglement structure of the trial state. This would be very interesting and deserves further study.

IV. DISCUSSION AND CONCLUSIONS

We have considered the concept of typicality to quantum critical points approached in PQMC simulations, where an initial state is, in effect, subject to an instantaneous quench followed by imaginary-time evolution with the critical Hamiltonian. The initial (trial) states can be thought as different temporal boundary conditions. Typicality here corresponds to an insensitivity of the universal critical fluctuations of the projected (evolved) state to the details of the initial state—even for trial states that are very poor in the variational sense—when the time τ of the evolution scales as $\tau = aL$.

By studying the bilayer Heisenberg model as an example, we have confirmed that the correct quantum-critical exponents are reproduced for a range of different trial states (supporting a complete independence on the trial state) and arbitrary factors a , after some cross-over system sizes that increases for decreasing a . While the correct critical exponents are always obtained for sufficiently large L , various non-universal numbers depend strongly on a even for $L \rightarrow \infty$.

While the typicality in the above sense is not too surprising, considering the similarity with $T > 0$ simulations where it is well known that one can scale the inverse temperature $\beta = bL^z$ to study quantum-critical scaling with the independent variable β eliminated, the freedom of choosing the trial state in projector simulations goes beyond the $T > 0$ formalism. Our purpose here has been

to confirm the typicality for a wide range of trial states, and also to make some observations that may be useful in practice. Beyond PQMC simulations, the typicality may also be very useful in calculations with tensor network states, where projection out of an initial state is often done in order to optimize the ground state. For studies of quantum critical points, it should be sufficient to project out to $\tau \propto L^z$ if z is known, and if z is not known it should also be possible to extract its value by studying the dependence of results on τ .

Naively, one might expect that it should always be better to choose a large factor a , so that the true ground state is projected out. However, our results, e.g., in Fig. 6, reveal that the leading finite-size scaling corrections, i.e., those governed by the exponent ω , can change sign as a is varied. This indicates the interesting and practically useful possibility that the leading corrections actually vanish at some special value of a . To make this point clearer, in Fig. 10, we show results obtained with the trial state $|\Psi_1\rangle$ and several values of a . Here we can see the change in sign of the correction very clearly, and it appears that $a \approx 0.3$ is the optimal value for canceling the leading correction. The corrections at this point would then be governed by the following correction exponent ω_2 . Since the amplitudes of the various scaling corrections are non-universal and also vary between different quantities, one may have to optimize a for each quantity of interest in order to take advantage of this effect, and for some quantities one may not even be able to find such an optimal values (and this may also depend on the trial state used). Thus, the method of optimizing the projection time may not be quite as powerful as the well known method of tuning an interaction in a model to reach a point at which the leading correction is absent for all quantities.²⁷ Nevertheless, this effect may potentially be very helpful in some cases. Moreover, apart from finding points where corrections are vanishing, it may also be useful in finite-size scaling studies to do common fits to results for several different values of a , since the mix of leading and subleading corrections depend strongly on a and the fits may become more stable with such information present in the data set. We are planning to explore these issues further in both PQMC and $T > 0$ simulations (where optimal prefactors b of the inverse temperature, $\beta = bL^z$, may exist).

ACKNOWLEDGMENTS

This work is supported by the National Natural Science Foundation of China under Grant No. 11734002 and 11775021 (W.G.), by the National Science Foundation under Grant No. DMR-1710170 (A.W.S.) and by a Simons Investigator Award (A.W.S.).

* sandvik@bu.edu

† waguo@bnu.edu.cn

- ¹ J. von Neumann, Z. Phys. **57**, 30 (1929); English translation, Eur. Phys. J. H **35**, 201 (2010).
- ² S. Goldstein, J. L. Lebowitz, R. Tumulka, and N. Zanghi, Phys. Rev. Lett. **96**, 050403 (2006).
- ³ S. Goldstein, J.L. Lebowitz, R. Tumulka, N. Zanghi, Eur. Phys. J. H **35**, 173, (2010).
- ⁴ M. Srednicki, Phys. Rev. E **50**, 888 (1994).
- ⁵ S. Sugiura and A. Shimizu, Phys. Rev. Lett. **108**, 240401 (2012).
- ⁶ S. Sugiura and A. Shimizu, Phys. Rev. Lett. **111**, 010401 (2013).
- ⁷ J. M. Deutsch, Phys. Rev. A **43**, 2046 (1991).
- ⁸ M. Rigol and M. Srednicki, Phys. Rev. Lett. **108**, 110601 (2012).
- ⁹ J. Jaklič and P. Prelovšek, Phys. Rev. B **49**, 5065 (1994).
- ¹⁰ J. Jaklič and P. Prelovšek, Adv. Phys. **49**, 1 (2000).
- ¹¹ S. R. White, Phys. Rev. Lett. **102**, 190601 (2009).
- ¹² S. Garnerone, T. R. de Oliveira, and P. Zanardi, Phys. Rev. A **81**, 032336 (2010).
- ¹³ S. Liang, Phys. Rev. B **42**, 6555 (1990).
- ¹⁴ A. W. Sandvik, Phys. Rev. Lett. **95**, 207203 (2005).
- ¹⁵ A. W. Sandvik and J. Kurkijärvi, Phys. Rev. B **43**, 5950 (1991).
- ¹⁶ A. W. Sandvik, AIP Conf. Proc. **1297**, 135 (2010).
- ¹⁷ L. Wang and A. W. Sandvik, Phys. Rev. B **81**, 054417 (2010).
- ¹⁸ Y.-R. Shu, S. Yin, and D.-X. Yao, Phys. Rev. B **96**, 094304 (2017).
- ¹⁹ K. Hida, J. Phys. Soc. Jpn. **59**, 2230 (1990); K. Hida, *ibid.* **61**, 1013 (1992).
- ²⁰ A. J. Millis and H. Monien, Phys. Rev. Lett. **70**, 2810 (1993).
- ²¹ A. W. Sandvik and D. J. Scalapino, Phys. Rev. Lett. **72**, 2777 (1994).
- ²² E. Manousakis, Rev. Mod. Phys. **63**, 1 (1991).
- ²³ S. Chakravarty, B. I. Halperin, and D. R. Nelson, Phys. Rev. Lett. **60**, 1057 (1988).
- ²⁴ A. V. Chubukov, S. Sachdev, and J. Ye, Phys. Rev. B **49**, 11919 (1994).
- ²⁵ S. Sachdev, *Quantum Phase Transitions*, 2nd edition (Cambridge University Press, Cambridge, England, 2011)
- ²⁶ L. Wang, K. S. D. Beach, and A. W. Sandvik, Phys. Rev. B **73**, 014431 (2006).
- ²⁷ M. Campostrini, M. Hasenbusch, A. Pelissetto, P. Rossi, and E. Vicari, Phys. Rev. B **65**, 144520 (2002).
- ²⁸ M. Matsumoto, C. Yasuda, S. Todo, and H. Takayama, Phys. Rev. B **65**, 014407 (2001).
- ²⁹ S. Wenzel, L. Bogacz, and W. Janke, Phys. Rev. Lett. **101**, 127202 (2008).
- ³⁰ F.-J. Jiang, Phys. Rev. B **85**, 014414 (2012).
- ³¹ L. Fritz, R. L. Doretto, S. Wessel, S. Wenzel, S. Burdin and M. Vojta, Phys. Rev. B **83**, 174416 (2011).
- ³² N. Ma, P. Weinberg, H. Shao, W. Guo, D.-X. Yao, and A. W. Sandvik, arXiv:1804.01273.
- ³³ S. Liang, B. Doucot, and P. W. Anderson, Phys. Rev. Lett. **61**, 365 (1988).
- ³⁴ A. W. Sandvik and H. G. Evertz, Phys. Rev. B **82**, 024407 (2010).
- ³⁵ J. Lou and A. W. Sandvik, Phys. Rev. B **76**, 104432 (2007).
- ³⁶ Yu-Cheng Lin, Y. Tang, J. Lou, and A. W. Sandvik, Phys. Rev. B **86**, 144405 (2012).
- ³⁷ We note that it was claimed in Ref. 38 that a wave function optimized and sampled by machine learning techniques can produce better energies than previously obtained variational energies for the 2D Heisenberg model. However, the far better variational results obtained in Ref. 36 were not included in the comparison.
- ³⁸ G. Carleo and M. Troyer, Science **355**, 602 (2017).
- ³⁹ K. S. D. Beach and A. W. Sandvik, Nucl. Phys. B **750**, 142 (2006).
- ⁴⁰ K. Binder, Phys. Rev. Lett. **47**, 693 (1981); Z. Phys. B: Condens. Matter **43**, 119 (1981).
- ⁴¹ E. L. Pollock and D. M. Ceperley, Phys. Rev. B **36**, 8343 (1987).
- ⁴² M. N. Barber, in *Phase Transitions and Critical Phenomena*, vol. 8, edited by C. Domb and J. Lebowitz (Academic, London, 1983).
- ⁴³ J. M. Luck, Phys. Rev. B **31**, 3069 (1985).
- ⁴⁴ H. Shao, W.-A. Guo, and A. W. Sandvik, Science **352**, 213 (2016).
- ⁴⁵ M. P. A. Fisher, P. B. Weichman, G. Grinstein, and D. S. Fisher, Phys. Rev. B **40**, 546 (1989).
- ⁴⁶ G. Kamieniarz and H. W. J. Blöte, J. Phys. A: Math. Gen. **26**, 201 (1993).
- ⁴⁷ S. Yasuda and S. Todo, Phys. Rev. E **88**, 061302(R) (2013).